ELSEVIER

International Journal of Solids and Structures 41 (2004) 3109–3124

INTERNATIONAL JOURNAL OF SOLIDS and STRUCTURES

www.elsevier.com/locate/ijsolstr

# Influence of the material constitutive models on the adiabatic shear band spacing: MTS, power law and Johnson–Cook models

L. Daridon [a], O. Oussouaddi [b], S. Ahzi [a,*]

[a] *IMFS-UMR 7507, Université Louis Pasteur, 2 Rue Boussingault, Strasbourg 67000, France*
[b] *LMCS, Department of Physics, FSTE, University My Ismaïl, Errachidia, Morocco*

Received 16 June 2003; received in revised form 10 December 2003

Available online 18 February 2004

**Abstract**

We propose to use the physically-based mechanical threshold stress (MTS) model for the analysis of adiabatic shear band spacing in HY-100 steel and Ti–6Al–4V alloy. Based on existing works, we use the perturbation method to determine the instability modes and their corresponding spacing. To validate our results, we compare them to those obtained using the phenomenological, and widely used, Johnson–Cook and power law models. We notice that the shear band spacing depends on the constitutive relation employed. We also compared the results from our analytical analysis to the available experimental ones. We show, for the first time, that the MTS model yields good results for adiabatic shear band spacing, particularly for the case of Ti–6Al–4V alloy.


*Keywords:* Shear band spacing; MTS model; Power law; Johnson–Cook model; Ti–6Al–4V

## 1. Introduction

The localization of plastic deformation in narrow bands (shear bands) is a major damage mechanism that occurs in ductile materials during high strain-rate deformation. They are observed in various applications such as metal forming, ballistic impact and high speed machining. Their formation signals a transition from a generally homogeneous deformation to a non-homogeneous one involving high strain gradients in a narrow region. In some circumstances many small bands may form throughout a volume of material (Nesterenko et al., 1995), in which case a general weakening occurs with the possibility of multiple failures and a general fragmentation. In other circumstances one band may dominate and material failure is restricted to just that one location. In the experiments of Marchand and Duffy (1988), thin-walled tubes were twisted at nominal strain rates in the range of 1200–1600 $s^{-1}$. Only one shear band is observed in their

* Corresponding author. Tel.: +33-390-242-952; fax: +33-399-244-972.
*E-mail address:* said.ahzi@ipst-ulp.u-strasbg.fr (S. Ahzi).

0020-7683/$ - see front matter © 2004 Elsevier Ltd. All rights reserved.
doi:10.1016/j.ijsolstr.2004.01.008

specimen. However, during the radial collapse of thick-walled cylinder deformed at a strain rate of $10^4$ $s^{-1}$, Nesterenko et al. (1995) observed 20 shear bands spaced about 0.85 and 1 mm in titanium and austenitic stainless steel, respectively.

Few numerical studies of the shear band spacing are available in the literature. Grady and Kipp (1987) have obtained the shear band spacing by accounting for momentum diffusion due to unloading within bands. Wright and Ockendon (1996) used a perturbation analysis to characterize a dominant mode, which corresponds to the most probable minimum spacing of shear bands. The analysis of Wright and Ockendon (1996) is restricted to the perfectly plastic materials. Linear perturbation analysis, which has been used in fluid mechanics, is first introduced in the context of adiabatic shear banding by Clifton (1978) and used later by Bai (1982), Molinari (1985), Shawki and Clifton (1989) among others (e.g. see Bai and Dodd, 1992). Wright and Ockendon (1996) postulated that, in an infinite body, perturbations growing at different sites will never merge and result in multiple shear bands. Thus, the wavelength of the dominant instability mode with the maximum growth rate will determine the shear band spacing. Molinari (1997) has extended Wright and Ockendon (1996) work to strain-hardening materials and has estimated the error in the shear band spacing due to the finite thickness of the block deformed in simple shear. Recently, Batra and Chen (2001) showed that four viscoplastic relations (Wright–Batra, Johnson–Cook, power law, and Bodner–Partom relation) gave quite different values for the shear band spacing and the bandwidth.

In this paper we adopted the multi-term mechanical threshold stress (MTS) model, which includes the superposition of different thermal activation barriers for dislocation motion, for adiabatic shear band spacing analysis. In this model, evaluation of work hardening associated with dislocation accumulation and recovery is principally based on the Voce law. To the best of our knowledge the MTS model has not been used in the literature for shear band spacing analysis. The MTS model is based on the dislocation concepts (Follansbee and Kocks, 1988) and was originally developed by Mecking and Kocks (1981). This model provides a better understanding of the plastic behavior under a wide range of strain rate. The system of governing equations for one-dimensional simple shearing deformation is formulated. For a given value of the strain, a perturbation of the fundamental solution is considered and the instability modes are determined. We used the postulate of Wright and Ockendon (1996) to determine the shear band spacing. To study the influence of the constitutive model on the results of the adiabatic shear band spacing, we compare the results from the Johnson and Cook (1983) and power law models to the results of the MTS model. We note that the shear band analysis using Johnson–Cook and power law are available in the literature (Batra and Chen, 2001; Molinari and Clifton, 1983; Klopp et al., 1985; Lee and Lin, 1998). The considered materials in this study are HY-100 steel and Ti–6Al–4V alloy. The capability of the MTS model to predict the shear band spacing is proven by comparison of our results to the experimental ones (Xue et al., 2002).

## 2. Governing equations

We consider the simple shear problem which models the torsional loading of a thin-walled tube. We use a plate with a finite thickness 2h in the $y$ direction whereas it is infinite in the shear direction $x$ and in the out-of-plane direction $z$ (see Fig. 1). We assume that the displacement is equal to zero in the $y$ direction and

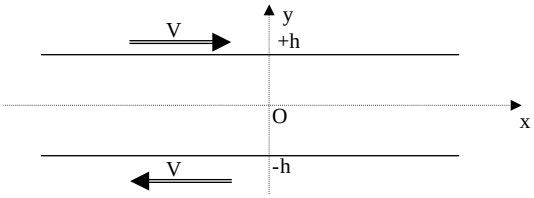


Fig. 1. Geometry used for shear analysis.

that all quantities are uniform along the $x$ and $z$ directions. Thus, the deformation field depends only on the space coordinate $y$. At the upper and lower surfaces, we apply a constant velocity parallel to the $x$ direction. The material is taken incompressible and its mass density is given by $\rho$. At large strain and high strain rate, the elastic effects can be ignored and adiabatic conditions can be assumed at the boundaries. Therefore, the governing equations are given by

- The momentum balance equation

$$\rho \frac{\partial v}{\partial t} = \frac{\partial \tau}{\partial y} \tag{1}$$

where $v$ is the component of the velocity along the $x$ direction (others component are equal to zero), $t$ is time and $\tau$ is the shear stress.

- The energy equation

$$\rho c \frac{\partial T}{\partial t} - k \frac{\partial^2 T}{\partial y^2} = \beta \tau \dot{\gamma} \tag{2}$$

where $T$ and $\dot{\gamma}$ are respectively the temperature and the shear strain rate. $c$ is the heat capacity, $k$ is the heat conductivity and $\beta$ is the Taylor–Quinney coefficient which describes the fraction of plastic work converted into heat.

- The compatibility equation

$$\dot{\gamma} = \frac{\partial v}{\partial y} \tag{3}$$

In order to complete the problem description we need to introduce a material constitutive relation expressed by the following general form:

$$\tau = \tau(\gamma, \dot{\gamma}, T, \phi) \tag{4}$$

where $\phi$ is an internal variable whose evolution is given by

$$\frac{\mathrm{d}\phi}{\mathrm{d}\gamma} = f(\phi, \tau, \dot{\gamma}, T) \tag{5}$$

The form of the function $f$ will vary with the specific constitutive relation.
The initial conditions are given by

$$v(y,0) = 0, \quad T(y,0) = T_{\mathrm{i}}, \quad \tau(y,0) = 0, \quad \phi(y,0) = 0 \tag{6}$$

where $T_{\mathrm{i}}$ is the initial temperature.
The boundary conditions considered here are:

- A constant velocity $V$ parallel to the shear direction is applied at the boundaries

$$v(-h,t) = -V, \quad v(h,t) = +V \quad \text{for } t \geqslant 0 \tag{7}$$

- As high strain rates are considered in this study, adiabatic conditions are assumed at the boundaries:

$$\frac{\partial T}{\partial y}(-h,t) = 0 \quad \text{and} \quad \frac{\partial T}{\partial y}(+h,t) = 0 \quad \text{for } t \geqslant 0 \tag{8}$$

## 3. Viscoplastic constitutive relations

It is well documented that the existence of a maximum on the stress–strain curve is a necessary condition for the occurrence of adiabatic shear band. This maximum is due to the competition between the stabilizing effect of the hardening and the strain rate and the destabilizing effect of the thermal softening. Therefore, we must use a viscoplastic relation which takes these three effects into account. In this study we will use the MTS model for the shear band spacing analysis. To highlight the efficiency of this model we also used two other constitutive relations Johnson–Cook (Johnson and Cook, 1983) and power law (Batra and Chen, 2001; Molinari and Clifton, 1983; Klopp et al., 1985) models and compared results from these models to the available experimental results.

### 3.1. The mechanical threshold stress model

The MTS model have initially been proposed by Kocks (1976), and then developed by Mecking and Kocks (1981), Estrin and Mecking (1984) and Follansbee and Kocks (1988). According to this model, the mechanical behavior of a material is only linked to the evolution of its microstructure. Thus, the kinetics of the plastic flow during loading is controlled by a unique structural parameter, $S$, which takes dislocation motion into account through an internal state variable, called MTS and denoted $\hat{\tau}$. This variable is defined as the flow stress at 0 K. We also note that the relation between the flow shear stress, denoted $\tau$, and the MTS depends on the material considered. In the following, we present the MTS model in the case of the HY-100 steel and Ti–6Al–4V alloy.

#### 3.1.1. HY-100 steel

For the HY-100 steel, the MTS is given by the following equation (Goto et al., 2000):

$$\hat{\tau} = \hat{\tau}_{\mathrm{a}} + \hat{\tau}_{\mathrm{i}} + \hat{\tau}_{\varepsilon} \tag{9}$$

where $\hat{\tau}_{\mathrm{a}} \equiv \tau_{\mathrm{a}}$ characterizes the rate-independent interactions of dislocations with long-range barriers, e.g. grain boundaries, $\hat{\tau}_{\mathrm{i}}$ characterizes the rate-dependent interactions of dislocations with short-range barriers due to solute and interstitial atoms and $\hat{\tau}_{\varepsilon}$ characterizes the rate-dependent interactions of dislocations with long-range barriers consisting of other dislocations and carbide particles. We note that $\hat{\tau}_{\varepsilon}$ increases during deformation by increasing dislocation density, which depends on temperature and strain rate because dynamic recovery takes place.

At different temperatures $T$ and shear strain rates $\dot{\gamma}$, the contributions to the flow shear stress $\tau_j$ are related to their reference counterparts $\hat{\tau}_j$ through the scaling functions $S_j(\dot{\gamma}, T)$ so that $\tau_j = S_j(\dot{\gamma}, T)\hat{\tau}_j$, where $j = i$ or $\varepsilon$. Hence, the flow shear stress $\tau$ is described as follows:

$$\tau = \tau_{\mathrm{a}} + S_{\mathrm{i}}(\dot{\gamma}, T)\hat{\tau}_{\mathrm{i}}\bar{\mu} + S_{\varepsilon}(\dot{\gamma}, T)\hat{\tau}_{\varepsilon}\bar{\mu} \tag{10}$$

where $\bar{\mu}$ is the normalized shear modulus for which the dependence on temperature is given by the following empirical relation (Varshni, 1970; Chen and Gray, 1996; Oussouaddi et al., 2003):

$$\bar{\mu} = \frac{\mu}{\mu_0} = 1 - \frac{D}{\mu_0 \exp\left(\frac{T_0}{T} - 1\right)} \tag{11}$$

Here $T_0$ and $D$ are empirical constants, $\mu$ is the shear modulus at $T$ and $\mu_0$ is the shear modulus at 0 K.

The scaling factor, $S_j(\dot{\gamma}, T)$, is derived from an Arrhenius expression relating strain rate to activation energy and temperature

$$\dot{\gamma} = \dot{\gamma}_{0j} \exp\left(-\frac{\Delta G_j}{kT}\right), \quad \text{where } \Delta G_j = g_{0j}\mu b^3 \left(1 - \left(\frac{\tau_j}{\hat{\tau}_j}\right)^{p_j}\right)^{q_j} \tag{12}$$

Table 1
MTS parameters for HY-100 steel (Bai and Dodd, 1992)

| Parameter | Value |
|---|---|
| $\tau_a$ [MPa] | 23.55 |
| $\hat{\tau}_i$ [MPa] | 779.65 |
| $\mu_0$ [GPa] | 71.46 |
| $D$ [MPa] | 2910 |
| $T_0$ [K] | 204 |
| $k$ [J/K] | 1.38E−23 |
| $b$ [m] | 2.48E−10 |
| $\dot{\gamma}_{0i}$ [$s^{-1}$] | 1E+13 |
| $g_{0i}$ | 1.161 |
| $q_i$ | 1.5 |
| $p_i$ | 0.5 |
| $\dot{\gamma}_{0\varepsilon}$ [$s^{-1}$] | 1E+7 |
| $g_{0\varepsilon}$ | 1.6 |
| $q_\varepsilon$ | 1 |
| $p_\varepsilon$ | 2/3 |
| $g_{0\varepsilon s}$ | 0.112 |
| $\dot{\gamma}_{0\varepsilon s}$ [$s^{-1}$] | 1E+7 |

where $\dot{\gamma}_{0j}$ is a reference shear strain rate, $k$ is the Boltzmann constant, $g_{0j}$ is a normalized activation energy, $b$ is the Burgers vector and $p_j$ and $q_j$ are statistical constants that characterize the shape of the obstacle profile ($0 \leqslant p_j \leqslant 1$, $1 \leqslant q_j \leqslant 2$, Mecking and Kocks, 1981). The scaling factor $S_j(\dot{\gamma}, T)$ can be derived from Eq. (12)

$$S_j(\dot{\gamma}, T) = \left\{ 1 - \left[ \frac{kT}{g_{0j}\mu b^3} \ln\left( \frac{\dot{\gamma}_{0j}}{\dot{\gamma}} \right) \right]^{1/q_j} \right\}^{1/p_j} \tag{13}$$

Plastic strain is implicitly represented through the term representing structure evolution $\hat{\tau}_\varepsilon$. The specific form for the expression of the plastic strain, $\gamma$, is dependent on the strain-hardening rate description. Voce law gives the strain-hardening response within the MTS model

$$\theta = \frac{\mathrm{d}\hat{\tau}_\varepsilon}{\mathrm{d}\gamma} = \theta_0 \left( 1 - \frac{\tanh\left( 2\frac{\hat{\tau}_\varepsilon}{\hat{\tau}_{\varepsilon s}} \right)}{\tanh(2)} \right) \tag{14}$$

where $\hat{\tau}_{\varepsilon s}$ is a temperature-and-rate-sensitive saturation shear stress, and $\theta_0$ is an experimentally determined stage II strain-hardening rate. The dependence of $\theta_0$ on temperature is determined by Goto et al. (2000), $\theta_0 = 5102.4 - 2.0758 \times T$ [MPa]. The saturation stress $\hat{\tau}_{\varepsilon s}$ is derived from the saturation threshold stress $\hat{\tau}_{\varepsilon s0}$ by

$$\ln\left( \frac{\dot{\gamma}_{\varepsilon s0}}{\dot{\gamma}} \right) = -\frac{g_{0\varepsilon s}\mu b^3}{kT} \ln\left( \frac{\hat{\tau}_{\varepsilon s}}{\hat{\tau}_{\varepsilon s0}} \right) \tag{15}$$

where $g_{0\varepsilon s}$ is normalized activation energy for dislocation–dislocation interactions.

The values of the material constants of the above-described model are listed in Table 1.

### 3.1.2. Ti–6Al–4V alloy

In the case of the Ti–6Al–4V alloy the flow stress is expressed by the following equation (Da Silva and Ramesh, 1997; Follansbee and Gray, 1989):

Table 2
MTS parameters for Ti–6Al–4V alloy (Molinari and Clifton, 1983)

| Parameter | Value |
|---|---|
| $\tau_a$ [MPa] | 58 |
| $\hat{\tau}_i$ [MPa] | 872 |
| $g_{0i}$ | 0.264 |
| $q_i$ | 2 |
| $p_i$ | 1 |
| $\dot{\gamma}_{0i}$ [$s^{-1}$] | 1E+10 |
| $g_{0s}$ | 0.8 |
| $\hat{\tau}_s$ [MPa] | 486.6 |
| $\dot{\gamma}_{0s}$ [$s^{-1}$] | 1E+10 |
| $\mu$ [GPa] | 49.02 |
| $q_s$ | 2 |
| $p_s$ | 1 |
| $g_{0\varepsilon}$ | 1.6 |
| $\dot{\gamma}_{0\varepsilon}$ [$s^{-1}$] | 1E+7 |
| $q_\varepsilon$ | 1 |
| $p_\varepsilon$ | 2/3 |
| $\hat{\tau}_{\varepsilon s}$ [MPa] | 310.62 |
| $b$ [m] | 2.55E−10 |
| $\theta_0$ [MPa] | 2721 |

Table 3
Physical parameters for HY-100 steel and Ti–6Al–4V alloy

| | $\rho$ [kg/m$^3$] | $c$ [J/kg K] | $k$ [W/m K] | $\beta$ |
|---|---|---|---|---|
| HY-100 | 7860 | 473 | 49.73 | 0.9 |
| Ti–6Al–4V | 4430 | 564 | 16 | 0.9 |

$$\tau = \tau_a + S_i(\dot{\gamma}, T)\hat{\tau}_i + S_s(\dot{\gamma}, T)\hat{\tau}_s + S_\varepsilon(\dot{\gamma}, T)\hat{\tau}_\varepsilon \tag{16}$$

where $\tau_a$ is an athermal component and $\hat{\tau}_i$, $\hat{\tau}_s$ and $\hat{\tau}_\varepsilon$ are respectively threshold stress due to interactions of dislocations due to interstitial atoms, to solute and to others dislocations. The specific form for the plastic strain, $\gamma$, depends on the hardening rate $\theta = d\hat{\tau}_\varepsilon/d\gamma$ given by the following empirical equation (Da Silva and Ramesh, 1997; Follansbee and Gray, 1989):

$$\theta = \frac{d\hat{\tau}_\varepsilon}{d\gamma} = \theta_0\left(1 - \frac{\hat{\tau}_\varepsilon}{\hat{\tau}_{\varepsilon s}}\right) \tag{17}$$

where $\hat{\tau}_{\varepsilon s}$ is the value of the saturation threshold stress, and $\theta_0$ is the hardening rate corresponding to the stage II and is experimentally determined (Da Silva and Ramesh, 1997). The values of the material constants of the above-described model for the Ti–6Al–4V alloy are listed in Table 2.

The physical parameters for both materials are given in Table 3.

### 3.2. Johnson–Cook model

Johnson and Cook (1983) proposed a phenomenological model for metals subjected to large strains, high strain rates and high temperatures. The Johnson–Cook model has enjoyed much success because of its simplicity and the availability of parameters of various materials of interest. The flow shear stress is given by

Table 4
Johnson–Cook parameters for HY-100 steel and Ti–6Al–4V alloy (Clifton, 1978; Klopp et al., 1985)

| | $\lambda_1$ [MPa] | $\lambda_2$ [MPa] | $\lambda_3$ | $\lambda_4$ | $\lambda_5$ | $\dot{\gamma}_0$ [$s^{-1}$] | $T_0$ [K] |
|---|---|---|---|---|---|---|---|
| HY-100 | 182.25 | 580.36 | 0.107 | 0.0227 | 0.7 | 3300 | 300 |
| Ti–6Al–4V | 418.4 | 394.4 | 0.47 | 0.035 | 1.0 | 1E−5 | 300 |

Table 5
Power law parameters for HY-100 steel (Clifton, 1978)

| | $\tau_0$ [MPa] | $\gamma_0$ | $\dot{\gamma}_0$ [$s^{-1}$] | $T_0$ [K] | $n\lambda_5$ | $m$ | $v$ |
|---|---|---|---|---|---|---|---|
| HY-100 | 405 | 0.012 | 3300 | 300 | 0.107 | 0.0117 | 0.75 |

$$\tau(\gamma,\dot{\gamma},T)=(\lambda_1+\lambda_2\gamma^{\lambda_3})\left(1+\lambda_4\ln\left(\frac{\dot{\gamma}}{\dot{\gamma}_0}\right)\right)\left(1-\left(\frac{T-T_0}{T_m-T_0}\right)^{\lambda_5}\right) \tag{18}$$

where $\gamma$ is the plastic shear strain, $\dot{\gamma}_0$ is a reference shear strain rate. $T_0$ and $T_m$ are respectively the initial or the reference temperature and the melting temperature. The coefficients $\lambda_1$, $\lambda_2$, $\lambda_2$, $\lambda_4$ and $\lambda_5$ are constitutive parameters. In the right hand side of Eq. (18), the first term gives the stress as a function of strain-hardening coefficient $\lambda_2$ and strain-hardening exponent $\lambda_3$, the second term represents instantaneous strain-rate sensitivity and the last term represents the temperature dependence of the flow stress. Here, $\lambda_4$ is the strain-rate parameter and $\lambda_5$ is the thermal-softening parameter.

For this model there is no internal variable. Therefore Eq. (5) reduces to $\phi = f = 0$. The Johnson–Cook model parameters for the HY-100 steel and Ti–6Al–4V alloy are given in Table 4.

### 3.3. Power law

In order to analyze the influence of each material parameter on the shear band spacing it is useful to use a constitutive relation with a simple form and decoupled terms for defining the strain hardening, strain-rate hardening and thermal softening behaviors of the material. Therefore, we used in this study the power law as reference behavior. Different authors (Molinari, 1985; Batra and Chen, 2001; Molinari and Clifton, 1983; Klopp et al., 1985) have described the stress–strain curves for dynamic loading by

$$\tau(\gamma,\dot{\gamma},T)=\tau_0\left(\frac{\gamma}{\gamma_0}\right)^n\left(\frac{\dot{\gamma}}{\dot{\gamma}_0}\right)^m\left(\frac{T}{T_0}\right)^v \tag{19}$$

where $\tau_0$ is the yield stress of the material in a quasi-static simple shear test, $n$ and $m$ characterize the strain and strain-rate hardening of the material and $v < 0$ characterizes its thermal softening. $\gamma_0$ is the strain at yield in a quasi-static simple shear test at $\dot{\gamma} = 10^{-4}\ s^{-1}$ and $\dot{\gamma}_0$ is a reference shear rate. $T_0$ is a reference temperature and $T$ is the current temperature. For the HY-100 steel the parameters data are given in Table 5.

## 4. Perturbation analysis

Linear perturbation methods were first introduced in the context of adiabatic shear banding by Clifton (1978). Here, we closely follow the work of Molinari (1997) in studying the stability of the homogeneous solution of the governing equations (1)–(5).

We consider the homogeneous solutions $\tau^{(0)}(t)$, $v^{(0)}(t)$, $\gamma^{(0)}(t)$, $T^{(0)}(t)$ for shear stress, velocity, shear strain and temperature respectively. Now we consider an infinitesimal perturbation of the homogeneous solution at time $t = t_0$ expressed by

$$\delta\mathbf{s}(y,t,t_0) = \delta\mathbf{s}^{(0)}\mathrm{e}^{\eta(t-t_0)}\mathrm{e}^{\mathrm{i}\xi y}, \quad t \geqslant t_0 \tag{20}$$

where $\delta\mathbf{s}^{(0)} = (\delta v^{(0)}, \delta\gamma^{(0)}, \delta\tau^{(0)}, \delta T^{(0)})$ and $y$ represents the position along the thickness of the plate. The quantities $\delta v^{(0)}$, $\delta\gamma^{(0)}$, $\delta\tau^{(0)}$ and $\delta T^{(0)}$ characterize the amplitude at time $t_0$ of the perturbation. The parameter $\xi$ is the wave number of the perturbation and $\eta$ is the inverse of the characteristic time, called growth rate of the perturbation. The fundamental solution is stable when the real part of $\eta$ is negative, $\mathrm{Re}(\eta) < 0$, and unstable when $\mathrm{Re}(\eta) > 0$.

The perturbed solution is defined by the following equation:

$$\mathbf{s}(y,t,t_0) = \mathbf{s}^{(0)}(y,t) + \delta\mathbf{s}(y,t,t_0) \tag{21}$$

Here, $s = (v, \gamma, \tau, T)$. By substituting the solution (Eq. (21)) into the governing equations (1)–(5) and linearizing provide, at time $t_0$, a linear set of equations for the amplitude $\delta\mathbf{s}^0$

$$\mathbf{A}(t_0,\eta,\xi)\cdot\delta\mathbf{s}^0 = 0 \tag{22}$$

This set of equation admits a non-trivial solution only if the determinant of the matrix $\mathbf{A}$ is equal to zero. This leads to a cubic equation for the growth rate $\eta$ of the perturbation

$$\begin{aligned}\rho^2 c\eta^3 + \rho\left(c\xi^2\frac{\partial\tau}{\partial\dot\gamma}\bigg|_{s^0} + k\xi^2 - \beta\dot\gamma^0\frac{\partial\tau}{\partial T}\bigg|_{s^0}\right)\eta^2 + \left(k\xi^2\frac{\partial\tau}{\partial\dot\gamma}\bigg|_{s^0} + \rho c\left(f^0\frac{\partial\tau}{\partial\phi}\bigg|_{s^0} + \frac{\partial\tau}{\partial\gamma}\bigg|_{s^0}\right) + \beta\tau^0\frac{\partial\tau}{\partial T}\bigg|_{s^0}\right)\xi^2\eta \\ + k\left(f^0\frac{\partial\tau}{\partial\phi}\bigg|_{s^0} + \frac{\partial\tau}{\partial\gamma}\bigg|_{s^0}\right)\xi^4 = 0\end{aligned} \tag{23}$$

In Eq. (23), partial derivatives are evaluated for the fundamental solution at time $t_0$. For given values of $\gamma^0 = \gamma^0(t_0)$ and $\xi$, three complex roots are obtained, $\eta_i(\xi,\gamma^0)$ $(i = 1, 2, 3)$. The root with the largest positive real part governs the instability of the homogeneous solution, and is hereafter referred to as the dominant instability mode, denoted $\eta_{\mathrm{D}}$.

The fundamental solution is such that the strain rate is uniform, $\dot\gamma^0 = \frac{V}{h}$. We note that in the case of power law, the heat equation (2) can be resolved analytically, with adiabatic assumption and where the constitutive law (13) is used to express the stress $\tau$. In the case of the Johnson–Cook model the temperature is obtained by numerical integration of the heat equation (2) where the constitutive law (7) is used to express the stress $\tau$. In the case of the MTS model the temperature is obtained by numerical integration of the heat equation (2) and the evolution equation of the internal variable (5). Then Eq. (4) is used to obtain the stress $\tau$.

## 5. Results and discussions

First, we study the influence of the constitutive relations (MTS, Johnson–Cook, power law) on the shear band spacing in the case of HY-100 steel and Ti–6Al–4V alloy. Then we compare our theoretical predictions with the experimental results of Xue et al. (2002) for Ti–6Al–4V alloy. At last, we also study the influence of the nominal shear strain rate and of some material parameters on the shear band spacing.

### 5.1. Influence of the constitutive relation on the shear band spacing

#### 5.1.1. Case of HY-100 steel

For the HY-100 steel modeled by three different constitutive relations (MTS, Johnson–Cook, power law), Fig. 2a–c shows the dominant growth rate, $\eta_D$, vs. the wave number, $\xi$, for various values of the average strain $\gamma^0$. These curves have been computed for a nominal strain rate $\dot{\gamma}^0 = 10^4$ s$^{-1}$ and an initial temperature $T_i = 300$ K. The dominant growth rate, $\eta_D$, depends on the initial time $t_0$ through the relation $\gamma^0 = \dot{\gamma}^0 t_0$. For each value of $\gamma^0$, the dominant growth rate increases for small values of the wave number until it reaches a maximum then decreases for large value of $\xi$. The existence of this maximum is characteristic of the dominant instability mode resulting from the competition of two stabilizing effects: inertia restrains the growth of long-wavelength modes (small $\xi$) while heat conduction restrains the growth of small-wavelength modes (large $\xi$). In what follows the maximum dominant growth rate at time $t_0$ for the perturbation is called the critical growth rate $\eta_c$, and the corresponding wave number is defined as the critical wave number $\xi_c$. A parametric study shows that the minimum value of the average strain required to

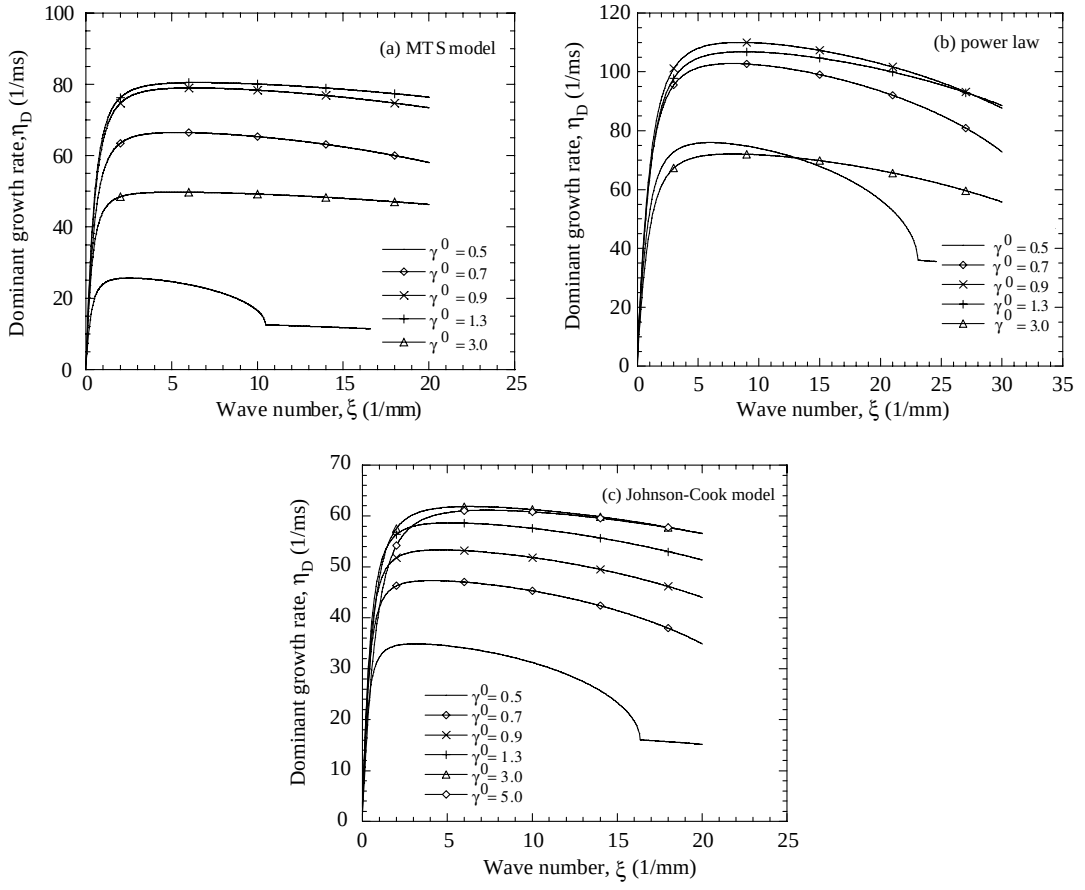


Fig. 2. (a) Dominant growth rate, $\eta_D$, vs. the wave number, in the case of the HY-100 steel and for the MTS model ($\dot{\gamma}^0 = 10^4$ s$^{-1}$, $T_i = 300$ K). (b) Dominant growth rate, $\eta_D$, vs. the wave number, in the case of the HY-100 steel and for the power law ($\dot{\gamma}^0 = 10^4$ s$^{-1}$, $T_i = 300$ K). (c) Dominant growth rate, $\eta_D$, vs. the wave number, in the case of the HY-100 steel and for the Johnson–Cook model ($\dot{\gamma}^0 = 10^4$ s$^{-1}$, $T_i = 300$ K).

obtain dominant growth rate instability is 0.32 for the power law model, 0.30 for the Johnson–Cook model and 0.448 for the MTS model, that is why we propose in Fig. 2 results for $\gamma^0 > 0.5$.

Fig. 3a–c shows the dependence of the critical growth rate $\eta_c$ and its corresponding wavelength $L_c = 2\pi/\xi_c$ on the average strain $\gamma^0$ for HY-100 steel. For both the power law and the MTS model, we observe that the curves of the critical growth rate and the critical wavelength vs. average strain have respectively a maximum $\eta_{cm}$ and a minimum $L_{cm}$. These values are obtained for two different values of the average strain, $\gamma_1^0$, $\gamma_2^0$

$$\eta_{cm} = \max_{\gamma^0 \geqslant 0} \eta_c(\gamma^0) = \eta_c(\gamma_1^0) \tag{24}$$

$$L_{cm} = \min_{\gamma^0 \geqslant 0} L_c(\gamma^0) = L_c(\gamma_2^0) \tag{25}$$

In the example considered here, since the values of $\gamma_1^0$ and $\gamma_2^0$ are very close for both the MTS and power law (Fig. 3a and b), we assume $\gamma_1^0 \cong \gamma_2^0$, which are equal to 1.05 and 1.1 respectively, for the power law and MTS

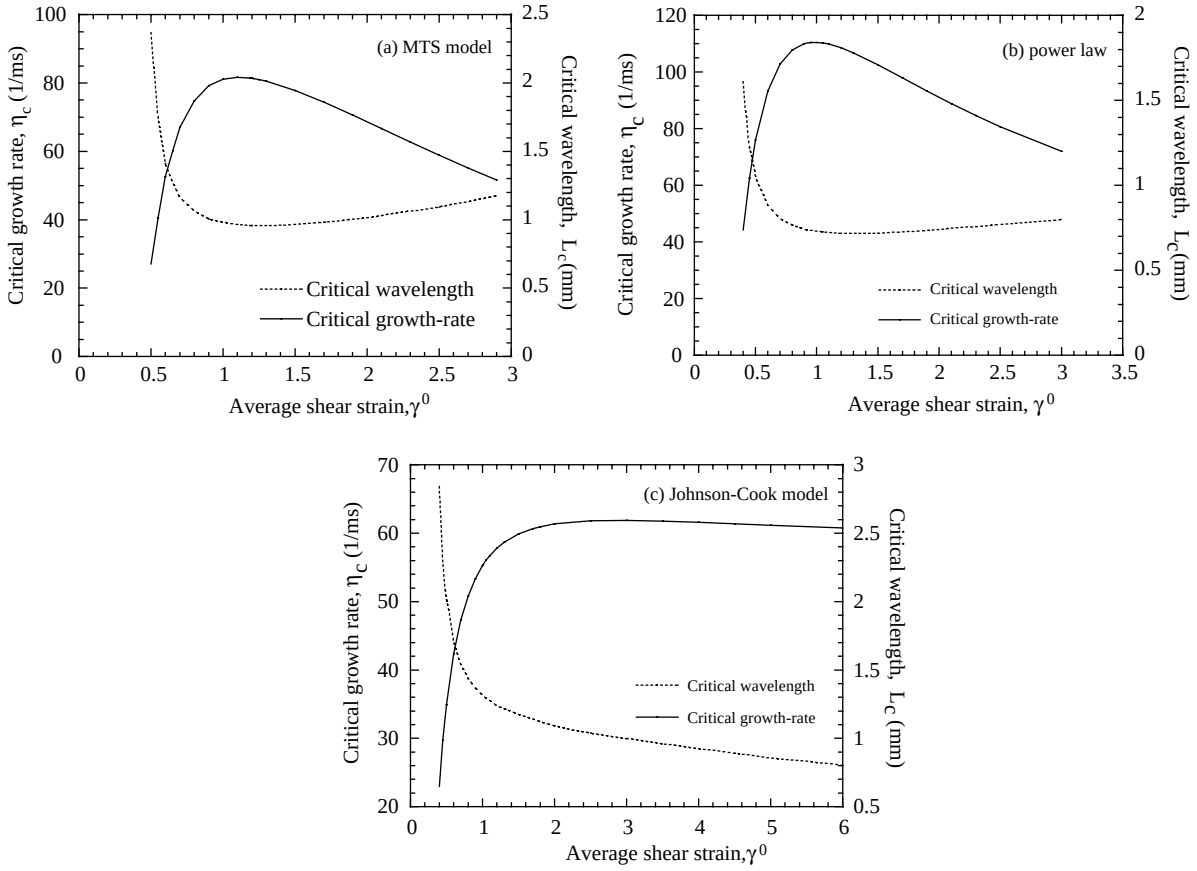


Fig. 3. (a) Influence of $\gamma^0$ on $\eta_c$ and $L_c$ for the HY-100 steel and the MTS model ($\dot{\gamma}^0 = 10^4$ s$^{-1}$, $T_i = 300$ K). (b) Influence of $\gamma^0$ on $\eta_c$ and $L_c$ for the HY-100 steel and the power law ($\dot{\gamma}^0 = 10^4$ s$^{-1}$, $T_i = 300$ K). (c) Influence of $\gamma^0$ on $\eta_c$ and $L_c$ for the HY-100 steel and the Johnson–Cook model ($\dot{\gamma}^0 = 10^4$ s$^{-1}$, $T_i = 300$ K).

models. This assumption is in a good agreement with the results obtained by Molinari (1997) in the case of XC18 steel with the power law model.

However, in the case of the Johnson–Cook model, the critical growth rate $\eta_c$ exhibits a maximum for $\gamma_1^0 = 2.875$, but the critical wavelength $L_c$ has no minimum value.

It the case of non-hardening materials, Wright and Ockendon (1996) postulated that the dominant instability mode with the maximum growth rate at time $t_0$ determines the shear band spacing, $L_s$

$$L_s = \frac{2\pi}{\xi_c(t_0^{\eta_c})} \tag{26}$$

where $t_0^{\eta_c}$ corresponds to the time at $\gamma_1^0$ . For strain-hardening materials, Molinari (1997) defined precisely the concept of critical time and corresponding strain $(t_0^{\eta_c}, \gamma_2^0)$ and postulated that the shear banding spacing is given by

$$L_s = L_{cm} \tag{27}$$

From our results, one can see that this latter postulate does not apply for the Johnson–Cook model (Figs. 3c and 5b). For the case of HY-100 steel, according to the definition (27), the shear band spacing will be essentially zero for the Johnson–Cook model whereas the definition (26) gives the value of 1.01 mm. For this material and for a nominal strain rate $\dot{\gamma}^0 = 10^4\ s^{-1}$, the shear band spacing obtained by the MTS model with the Wright and Ockendon (1996) and Molinari (1997) definitions are respectively equal to 0.97 and 0.96 mm. Using the power law, these values are respectively equal to 0.73 and 0.72 mm. These results show that both definitions give essentially the same $L_s$ values for each of the two models, MTS and power law. We note that these results for HY-100 steel are in good agreement with Molinari's results obtained for the case of XC18 steel using the power law model. However, Chen and Batra's (1999) work indicates that these two definitions lead to quite different values of the shear band spacing when the material is modeled by an affine function for the temperature rise.

According to the above remarks, Eq. (26) is more adequate and it is used in the following to determine the adiabatic shear band spacing. The results obtained by the three models for $L_s$ using this equation (0.73 mm for the power law, 0.97 mm for the MTS and 1.01 mm for the Johnson–Cook) are slightly different and they are in an acceptable order in comparison with the results presented in the literature, particularly those of Nesterenko et al. (1995) where they observed approximately 32 shear bands regularly separated by 1 mm in the case of an austenitic stainless steel. This experimental result corresponds to a rather developed stage of self-organization of processes of shear bands. In another paper of Nesterenko et al. (1998), a different experimental set up was used to allow the investigation of the initial stage of nucleation and self-organization of nuclei of shear bands. In this work, Nesterenko et al. (1998) reported a much lower shear band spacing, 0.12 mm, for the 304L stainless steel corresponding to 235 shear band nuclei. Stainless-steel data and details on the experimental and theoretical work on the collective behavior of shear bands may be found in the work of Nesterenko (2001). We note that a similar relation to (26) was suggested by Bai (1982) defining the characteristic length as $\frac{1}{\xi(t_0^{\eta_c})}$ which leads to a smaller value of the shear band spacing than the one we suggest using Eq. (26).

### *5.1.2. Case of Ti–6Al–4V alloy*

For the Ti–6Al–4V alloy modeled by two different constitutive relations (MTS, Johnson–Cook), Fig. 3a and b shows the dominant growth rate, $\eta_D$, vs. the wave number, $\xi$, for various values of the average strain $\gamma^0$. These curves have been computed for a nominal strain rate $\dot{\gamma}^0 = 10^4\ s^{-1}$ and an initial temperature $T_i = 300$ K. As in the case of the HY-100 steel, the dominant growth rate, $\eta_D$, (Fig. 4a and b) increases for small values of the wave number until it reaches a maximum then decreases for large value of $\xi$. We notice that the Johnson–Cook model need to introduce, for a given nominal strain rate, the perturbation latter than with the MTS model. Fig. 5a and b shows the dependence of the critical growth rate $\eta_c$ and its

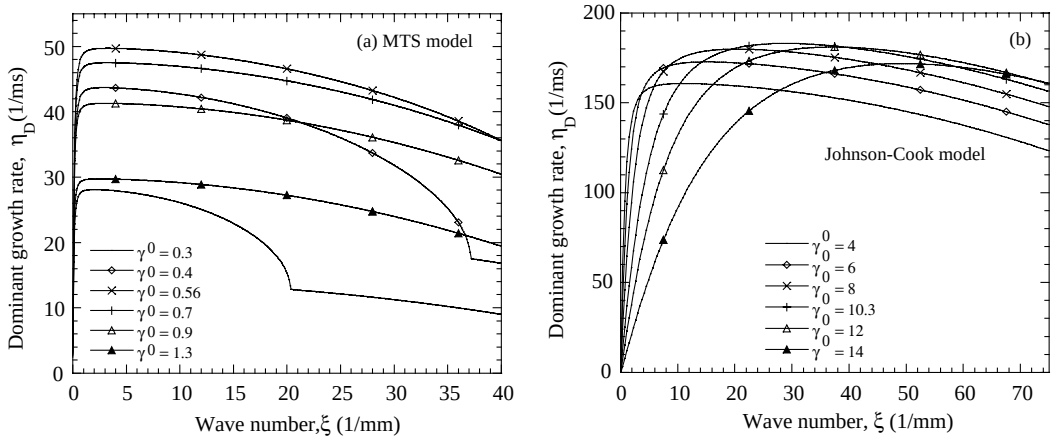


Fig. 4. (a) Dominant growth rate, $\eta_D$, vs. the wave number, in the case of the Ti–6Al–4V alloy and for the MTS model ($\dot{\gamma}^0 = 10^4$ s$^{-1}$, $T_i = 300$ K). (b) Dominant growth rate, $\eta_D$, vs. the wave number, in the case of the Ti–6Al–4V alloy and for the Johnson–Cook model ($\dot{\gamma}^0 = 10^4$ s$^{-1}$, $T_i = 300$ K).

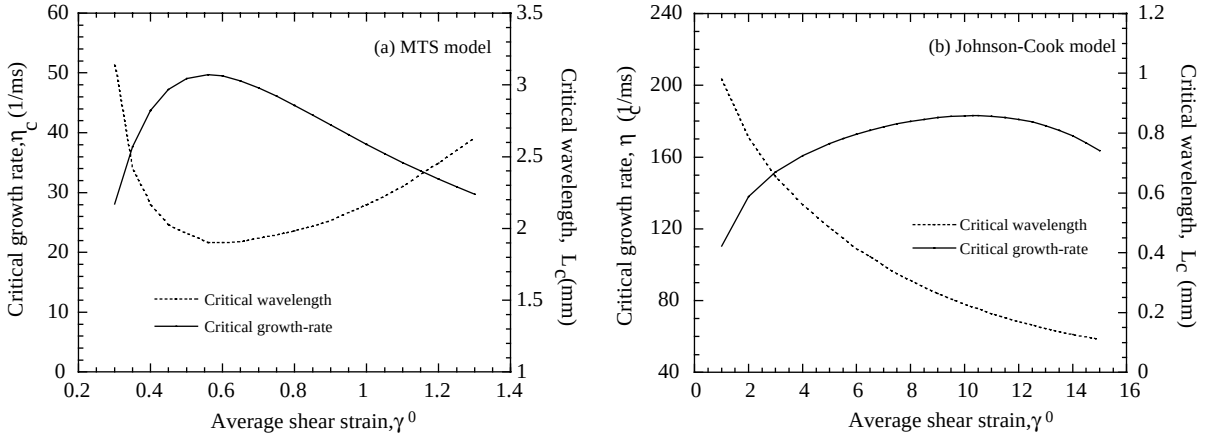


Fig. 5. (a) Influence of $\gamma^0$ on $\eta_c$ and $L_c$ for the HY-100 steel and the MTS model ($\dot{\gamma}^0 = 10^4$ s$^{-1}$). (b) Influence of $\gamma^0$ on $\eta_c$ and $L_c$ for the HY-100 steel and the Johnson ($\dot{\gamma}^0 = 10^4$ s$^{-1}$).

corresponding wavelength $L_c = 2\pi/\xi_c$ on the average strain $\gamma^0$ for Ti–6Al–4V alloy. In the case of the Johnson–Cook model (Fig. 5b), the critical growth rate $\eta_c$ exhibits a maximum for $\gamma_1^0 = 10$, but the critical wavelength $L_c$ has no minimum value as for the HY-100 steel. However for the Ti–6Al–4V alloy, the curves (Fig. 5a) $\eta_c$ vs. $\gamma^0$ and $L_c$ vs. $\gamma^0$ exhibit respectively a maximum, $\gamma_1^0 = 0.56$, and a minimum, $\gamma_2^0 = 0.57$. This observation supports the choice of Eq. (26) as definition of critical growth rate $\eta_c$.

To show the capability of the MTS model to predict the shear band spacing, we now compare our theoretical predictions, for the Ti–6Al–4V alloy, to experimental results available in the literature (Xue et al., 2002). Here we consider three constitutive models, MTS, Johnson–Cook and Xue et al. (2002), and we use the Wright–Ockendon definition (Eq. (26)) to calculate the shear bands spacing, $L_s$. In our calculation, we adopted the experimental loading conditions. The nominal shear strain rate is taken to be $6\times10^4$ s$^{-1}$ and the initial temperature is equal to 300 K. It should be noted that theoretical results of Xue et al.

Table 6
Comparison of theoretical and experimental results for adiabatic shear band spacing for Ti–6Al–4V alloy

| | Experimental value | Theoretical value obtained by Xue et al. (2002) | Theoretical value obtained with Johnson–Cook law | Theoretical value obtained with MTS model |
|---|---|---|---|---|
| $L_s$ (mm) | 0.53 | 0.1 | 0.02 | 0.52 |

(2002) were obtained using a power law-based constitutive relation characterized by a linear thermal softening

$$\tau = \alpha_0(\gamma + \gamma_i)^n \dot{\gamma}^m (1 - aT) \tag{28}$$

where $\alpha_0$ and $a$ are constants.

Our theoretical predictions for the shear band spacing obtained by the MTS and the Johnson–Cook models are compared with the theoretical and experimental results of Xue et al. (2002) in Table 6. We note that the power law with linear softening (Eq. (28)) and the Johnson–Cook models lead to results far away from the experimental result in the case of the Ti–6Al–4V alloy (see Table 6). Indeed the experimental value is five times the theoretical value obtained using the power law with linear softening and 20 times the value obtained with the Johnson–Cook model. On the other hand, the theoretical value obtained by the MTS model is very close to the experimental one. Consequently, we can conclude that on one hand the shear band spacing depends on the constitutive relation, and on the other hand the MTS model gives a much better results in comparison to the two phenomenological laws in the case of the Ti–6Al–4V alloy.

### 5.2. Influence of the strain rate (loading rate)

Fig. 6 represents the dependence of the shear band spacing on the nominal shear strain rate, $\dot{\gamma}^0$, in the case of HY-100 steel for the power law (Eq. (19)), the Johnson–Cook and the MTS models. For each one of these models, the shear band spacing rapidly decreases with an increase of the nominal strain rate until about $\dot{\gamma}^0 = 2 \times 10^4\ s^{-1}$, beyond which results show a tendency for the shear band spacing to saturate. We also note that the difference between the theoretical predictions obtained by the three models is more important for low nominal shear strain. For instance, at $\dot{\gamma}^0 = 10^3\ s^{-1}$ the shear bands spacing is equal to 4.7389, 4.0513 and 5.7074 mm, for the MTS, the power law and of the Johnson–Cook models respectively.

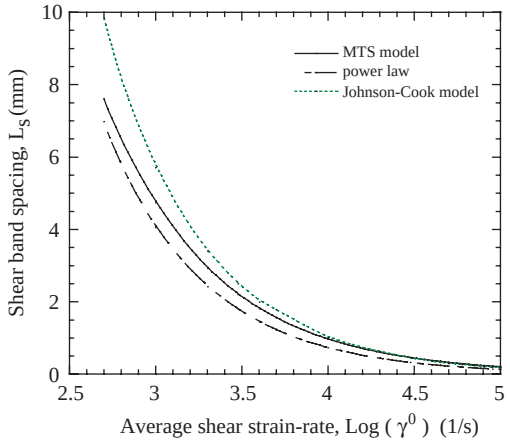


Fig. 6. Influence of the nominal strain rate on the shear band spacing, $L_s$, for the HY-100 steel.

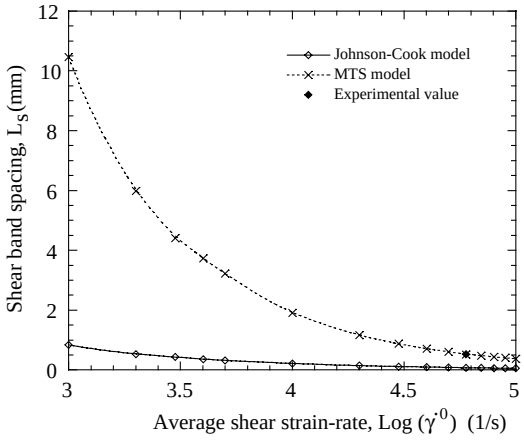


Fig. 7. Influence of the nominal strain rate on the shear band spacing, $L_s$, for the Ti–6Al–4V alloy.

On the other hand at $\dot{\gamma}^0 = 10^5\ s^{-1}$ $L_s$ is equal to 0.20516, 0.13483 and 0.17952 mm, for the MTS, the power law and the Johnson–Cook models respectively.

In the case of Ti–6Al–4V alloy, Fig. 7 illustrates the influence of the nominal shear strain rate on the shear band spacing. We note that the material parameters for the power law are not available in the literature. Therefore, the calculations are limited here to the case of the Johnson–Cook and the MTS models only. The results obtained by the MTS model are in agreement with the limited experimental result available in the literature (Xue et al., 2002). Due to the choice of the $L_s$ definition and to the formulation of the MTS model, we are unable to provide an analytical relation between the shear band spacing and the strain rate to describe Fig. 7.

### 5.3. Influence of thermal conductivity

To investigate the influence of the thermal conductivity on the shear band spacing, we considered a nominal shear strain rate $\dot{\gamma}_0 = 10^4\ s^{-1}$ and an initial temperature $T_i = 300$ K. In Fig. 8, we show the vari-

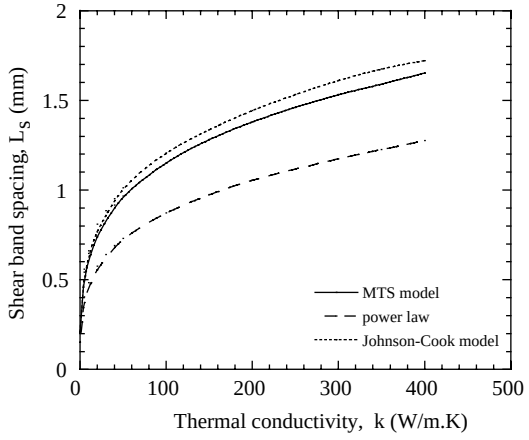


Fig. 8. Influence of the thermal conductivity on the shear band spacing, $L_s$.

ation of the shear band spacing $L_s$ in terms of the thermal conductivity $k$ for the power law, the MTS and the Johnson–Cook models. The effect of conductivity is shown to be significant for the three models. In this part, several values of conductivity were considered, the other parameters remaining constant and correspond to those of HY-100 steel. The shear band spacing $L_s$ increases monotonically with an increase in $k$. This is in accord with the known stabilizing effect of the thermal conductivity. However, the shear band spacing obtained by the MTS model is larger than that obtained by the power law and the gap between the two predictions increases with thermal conductivity coefficient. The shear band spacing obtained by the power law is the smallest and that obtained by the Johnson–Cook model is the largest for all values of $k$.

## 6. Conclusions

We proposed the use of the MTS model along with the use of the perturbation method for the analysis of shear band spacing in the case of HY-100 steel and Ti–6Al–4V alloy. The MTS model describes the evolution of the flow stress based on dislocation concepts. This model provides a better description of the flow behavior for a large range of strain rates including low and high strain rates. The use of this model requires a numerical solution of the heat equation (2) and the evolution equation of the internal variable $\hat{\tau}_e$. However, in existing works on the analysis of shear band spacing, the used models for the flow stress such as the power law lead to an analytical solution for the heat equation. In order to compare to existing analyses, we used the power law and the Johnson–Cook models. Results from the MTS model have the same trends as the power law as well as other used models in the literature. However, the predicted result for adiabatic shear band spacing by the MTS model seems to be in a better agreement with the experimental results than the results of the simple power law and Johnson–Cook models. We have therefore shown that the MTS model predicts well the value of the shear band spacing, and the influence of strain rate and thermal conductivity on this value. Strain rate has a destabilizing effect whereas thermal conductivity has a stabilizing effect.

## References

Bai, Y.L., 1982. Thermo-plastic instability in simple shear. J. Mech. Phys. Solids 30, 195–207.

Bai, Y.L., Dodd, B., 1992. Adiabatic Shear Localization: Occurrence, Theories and Applications. Pergamon Press, Oxford.

Batra, R.C., Chen, Li, 2001. Effect of viscoplastic relations on the instability strain, shear band initiation strain, the strain corresponding to the minimum shear band spacing, and the band width in a thermoviscoplastic material. Int. J. Plasticity 17, 1465–1489.

Chen, L., Batra, R.C., 1999. Effect of material parameters on shear band spacing in work-hardening gradient dependent thermoviscoplastic materials. Int. J. Plasticity 15, 551–574.

Chen, S.R., Gray, G.T., 1996. Constitutive behavior of tantalum and tantalum–tungsten alloys. Metall. Mater. Trans. A 27A, 2994–3006.

Clifton, R.J., 1978. Adiabatic shear in material response to ultra loading rates. Report No. NMAB-356. National Advisory Board Committee, pp. 129–142 (Chapter 8).

Da Silva, M.G., Ramesh, K.T., 1997. The rate-dependent deformation and localization of fully dense and porous Ti–6Al–4V. Mater. Sci. Eng. 232, 11–22.

Estrin, Y., Mecking, H., 1984. A unified phenomenological description of work hardening and creep based on one-parameter models. Acta. Metall. 32, 57–70.

Follansbee, P.S., Gray, G.T., 1989. An analysis of the low temperature low and high strain rate deformation of Ti–6Al–4V. Metall. Trans. A 20, 863–874.

Follansbee, P.S., Kocks, U.F., 1988. A constitutive description of the deformation of copper based on the use of the mechanical threshold as an internal state variable. Acta Metall. 36, 81–93.

Goto, D.M., Bingert, J.F., Chen, S.R., Gray, G.T., Garrett, R.K., 2000. The mechanical threshold stress constitutive-strength model description of HY-100 steel. Metall. Mater. Trans. 31A, 1985–1996.

Grady, D.E., Kipp, M.E., 1987. The growth of unstable thermoplastic shear with application to steady wave shock compression in solids. J. Mech. Phys. Solids 35, 95–118.

Johnson, G.R., Cook, W.H., 1983. A constitutive model and data for metals subjected to large strains, high strain rates and high temperatures. In: Proceedings of 7th International Symposium on Ballistics, The Hague, Netherlands, pp. 12–21.

Klopp, R.W., Clifton, R.J., Shawki, T.G., 1985. Pressure-shear impact and the dynamic viscoplastic response of metals. Mech. Mater. 4, 375–385.

Kocks, U.F., 1976. Laws for work-hardening and low temperature creep. ASME J. Eng. Mater. Technol. 98, 76–85.

Lee, W.S., Lin, C.F., 1998. Plastic deformation and fracture behavior of Ti–6Al–4V alloy loaded with high strain rate under various temperatures. Mater. Sci. Eng. A 241, 48–59.

Marchand, A., Duffy, J., 1988. An experimental study of the formation process of adiabatic shear bands in a structural steel. J. Mech. Phys. Solids 36, 251–283.

Mecking, H., Kocks, U.F., 1981. Kinetics of flow and strain-hardening. Acta Metall. 29, 1865–1875.

Molinari, A., 1985. Instabilité thermo-visco-plastique en cisaillement simple. J. Méc. Théor. Appl. 4, 659–684.

Molinari, A., 1997. Collective behavior and spacing of adiabatic shear bands. J. Mech. Phys. Solids 45, 1551–1575.

Molinari, A., Clifton, R., 1983. Résultats exacts en théorie non liniéare. Compt. Rend. Acad. Sci. II, 1–4.

Nesterenko, V.F., 2001. Dynamiics of Heterogeneous Materials. Springer Verlag, New York.

Nesterenko, V.F., Meyers, M.A., Wright, T.W., 1995. Collective behavior of shear bands. In: Murr, L.E., Staudhammer, K.P., Meyers, M.A. (Eds.), Metallurgical and Materials Application of Shock-Wave and High-Strain-Rate Phenomena. Elsevier Science, Amsterdam, pp. 397–404.

Nesterenko, V.F., Meyers, M.A., Wright, T.W., 1998. Self-organisation in the initiation of adiabatic shear bands. Acta Metall. 46 (1), 327–340.

Oussouaddi, O., Daridon, L., Ahzi, S., Bouami, D., 2003. Application of the mechanical threshold stress for the analysis of the shear band spacing. Rev. Méc. Appl. Théor. 1 (4), 239–252.

Shawki, T.G., Clifton, R.J., 1989. Shear band formation in thermal viscoplastic materials. Mech. Mater. 8, 13–43.

Varshni, Y.P., 1970. Temperature dependence of the elastic constants. Phys. Rev. B 2, 3952–3958.

Wright, T.W., Ockendon, H., 1996. A scaling law for the effect of inertia on the formation of adiabatic shear bands. Int. J. Plasticity 12, 927–934.

Xue, Q., Meyers, M.A., Nesterenko, V.F., 2002. Self-organization of shear bands in titanium and Ti–6Al–4V alloy. Acta Mater. 50, 575–596.